Surface recombination in ZnO nanorods grown by chemical bath deposition

Q. X. Zhao, L. L. Yang, M. Willander, B. E. Sernelius and P. O. Holtz

Original publication:

Q. X. Zhao, L. L. Yang, M. Willander, B. E. Sernelius and P. O. Holtz, Surface recombination in ZnO nanorods grown by chemical bath deposition, 2008, Journal of Applied Physics, (104), 073526.
http://dx.doi.org/10.1063/1.2991151.

Surface recombination in ZnO nanorods grown by chemical bath deposition

Q. X. Zhao,[1,a)] L. L. Yang,[1] M. Willander,[1] B. E. Sernelius,[2] and P. O. Holtz[2]
[1]*Department of Science and Technology, Linköping University, Campus Norrköping, SE-601 74 Norrköping, Sweden*
[2]*Department of Physics, Chemistry and Biology, Linköping University, SE-581 83 Linköping, Sweden*

(Received 27 June 2008; accepted 12 August 2008; published online 8 October 2008)

Vertically well-aligned ZnO nanorods on Si substrates were prepared by a two-step chemical bath deposition (CBD) method. The optical properties of the grown ZnO nanorods were investigated by time resolved photoluminescence spectroscopy. It was found that the effective decay time of the near bandgap recombination in the CBD grown ZnO nanorods strongly depends on the diameter of the ZnO nanorods. Typically, the decay curves obtained from these ZnO nanorods show a combination of two exponential decays. The experimental results show that the fast exponential decay is related to the surface recombination and the slow decay is related to the "bulk" decay. The measured decay time of the effective surface recombination decreases with decreasing diameter, while the bulk decay time remains unchanged. The results also show that an annealing treatment around 500 °C significantly reduces the surface recombination rate. A simple carrier and exciton diffusion equation is also used to determine the surface recombination velocity, which results in a value between 1.5 and 4.5 nm/ps. © *2008 American Institute of Physics*. [DOI: 10.1063/1.2991151]

I. INTRODUCTION

ZnO is a major potential candidate for optoelectronic applications due to its wide bandgap energy of 3.37 eV at room temperature and large exciton binding energy (60 meV). For the past ten years, ZnO epilayer, ZnO nanorods, and various ZnO nanostructures have been grown by various techniques, including molecular beam epitaxy,[1–4] metal organic vapor phase epitaxy or metal organic chemical vapor deposition,[5–10] pulsed laser deposition,[11,12] vapor-liquid-solid (VLS) catalytic growth technique,[13–15] magnetron sputtering,[16] and chemical bath deposition (CBD).[17–19] A major advantage for ZnO nanostructures, e.g., nanowires and nanorods, is that they can be easily grown on various substrates and nonlattice materials including flexible polymers. In addition, ZnO nanorods can be advantageous with a low density of defects. The growth of defect-free structures is more likely for nanorods in comparison with epilayers, since the strain in the nanorods can be efficiently relieved by elastic relaxation at the free lateral surfaces rather than by plastic relaxation. ZnO nanostructures have been widely investigated by cathodoluminescence[20] and photoluminescence (PL) at room temperature[15,21] and low temperature.[22–24] However, the investigations by low temperature time resolved PL spectroscopy of ZnO nanorods are limited.[25,26] One of the significant differences between nanorods and an epilayer is the larger surface area of the former. This large surface area can be an advantage for some applications, for example, sensor devices. However, it can also be a problem in other applications, for example, optoelectronic devices such as light emitting diodes and solar-cell devices, since the surface recombination rate may become dominating, resulting in a short carrier lifetime. So far, the knowledge about surface recombination in ZnO nanorods is limited.

In this paper, we present an optical investigation of ZnO nanorods with different diameters grown by the CBD method. The surface effect versus the diameter of the ZnO nanorods was studied by means of time resolved PL for the first time to the best of our knowledge. The results clearly illustrate that the surface recombination becomes a dominating recombination channel with a decreasing diameter of the ZnO nanorods. The results also indicate that the surface recombination rate can be suppressed in ZnO nanorods with a mild thermal treatment at 500 °C.

II. EXPERIMENTS

The ZnO nanorods used in this investigation were grown on Si substrates by the CBD method, which includes a two-step process, i.e., a substrate treatment prior to the CBD growth. The pretreatment of the substrates, by coating the substrate with a solution of zinc acetate dihydrate ($Zn(C_2H_3O_2)_2 \cdot 2H_2O$) dissolved in pure ethanol with a concentration of 5 mM, was used to control the diameter of ZnO nanorods. In the CBD growth, the aqueous solutions of zinc nitrate hexahydrate [$Zn(NO_3)_2 \cdot 6H_2O$, 99.9% purity] and methenamine ($C_6H_{12}N_4$, 99.9% purity) were first prepared and mixed together. The concentrations of both were fixed at 0.1*M*. The pretreated Si substrates were immersed into the aqueous solution, and ZnO was grown at an elevated temperature of 93 °C. The major problems in the CBD growth are the reproducibility, the size control, and the density of the ZnO nanorods. These problems have been solved in our recent investigations and, e.g., by controlling the precoating layer thickness, the reproducibility and the ZnO nanorod size and density can be controlled.[27] Three samples containing ZnO nanorods on Si (001) substrates with diameters of 150,

a)Electronic mail: Qingxiang.Zhao@itn.liu.se.

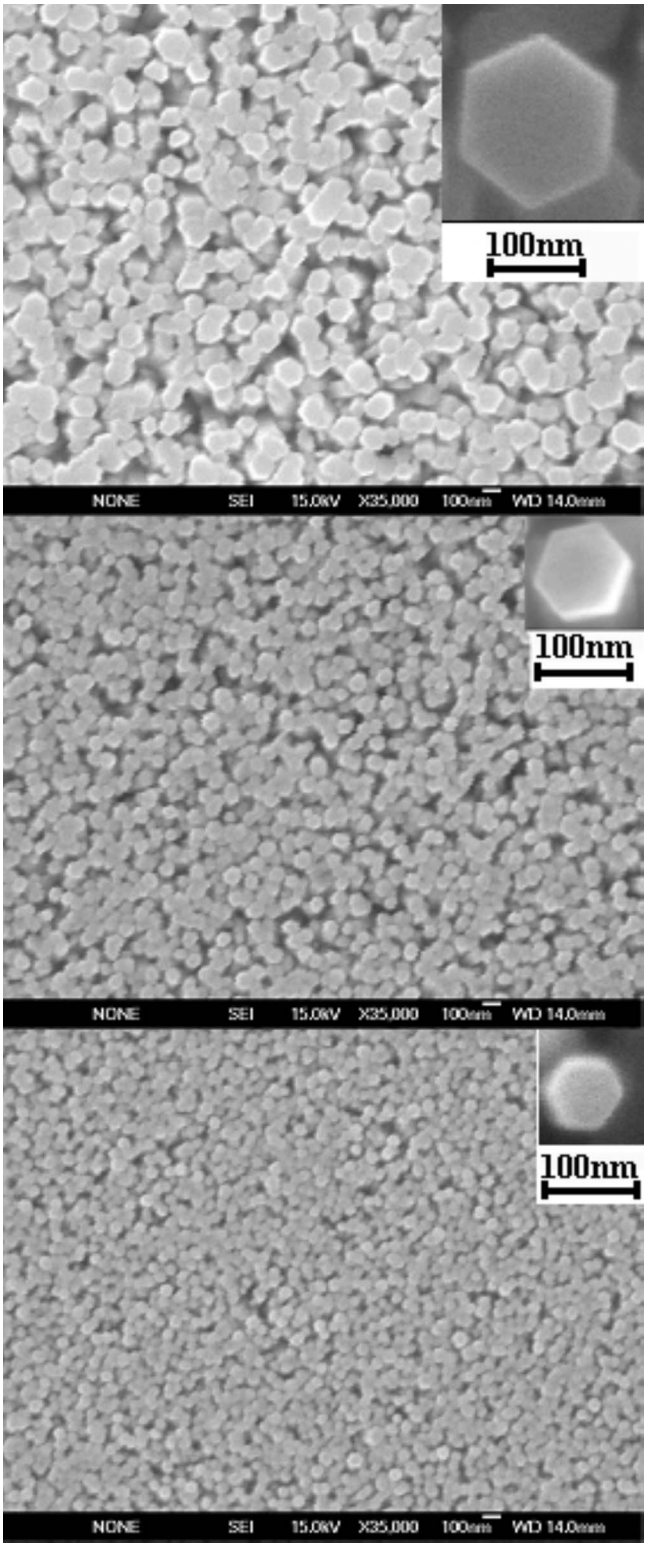

FIG. 1. Top SEM images for ZnO nanorods with different average diameters, i.e., 150, 90, and 60 nm. Insets show a highly magnified top image of a single ZnO nanorod for each sample.

90, and 60 nm, respectively, were used in this study. Scanning electron microscopy (SEM) images of these structures are shown in Fig. 1. The ZnO nanorods were vertically aligned on the Si (001) substrates. For the ZnO nanorod sample with a diameter of 90 nm, a postgrowth thermal treatment was performed at 500 °C for 60 min in air atmosphere.

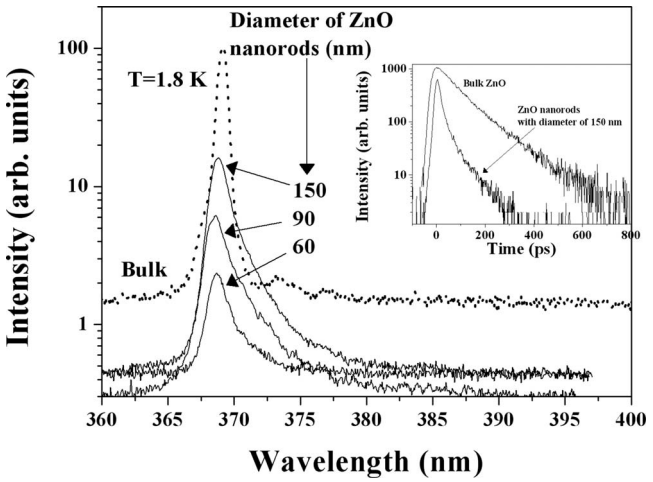

FIG. 2. PL spectra for as-grown ZnO nanorods with different diameters (150, 90, and 60 nm) measured at 1.8 K. A PL spectrum from bulk ZnO is also included for comparison. The inset shows the decay curves for bulk ZnO and ZnO nanorods with a diameter of 150 nm.

Time resolved PL was performed by using an excitation laser line from a frequency tripled sapphire:Ti laser emitting at 266 nm with a 200 fs pulse width and a 80 MHz repetition rate. The luminescence signal is dispersed by a 0.3 m monochromator and time resolved by a streak camera. The spectral resolution is about 1 meV and the time resolution is 7 ps. The measurements were done under weak excitation conditions ($0.5\ \mathrm{W/cm^2}$). The PL signals presented in the following were recorded at 1.8 K.

III. RESULTS AND DISCUSSIONS

Figure 2 shows the time integrated PL spectra of the CBD grown ZnO nanorods with different diameters. The PL spectrum from a bulk ZnO sample (from Universitywafer and grown by the hydrothermal method) was included in the same figure for comparison. The PL spectra are similar for all samples, i.e., a dominating emission of donor bound excitons. By examining the PL spectra, it is obvious that the exciton emission from the ZnO nanorods has a low energy tail in comparison with the corresponding emission in the bulk ZnO. This indicates that this PL band contains more than one bound exciton. The integrated intensity of the PL peak decreases with decreasing diameter of the ZnO nanorods. The inset of Fig. 2 shows the decay curves with the detection energy at the maximum of the PL peak for the bulk ZnO and the 150 nm ZnO nanorods, respectively. It clearly demonstrates the difference between the ZnO nanorods and the bulk ZnO layer. The decay curve from the bulk ZnO shows a single exponential time decay, while the ZnO nanorods exhibit a nonexponential decay. As earlier demonstrated for Si epilayer,[28–30] the surface recombination can strongly influence the decay time. The excess minority carriers via the near bandgap recombination exhibit a single exponential decay or a nonexponential decay, depending on whether the surface recombination is the major recombination channel or not. The surface recombination is characterized by two parameters, i.e., surface recombination velocity S and carrier diffusion length D. The influence of the surface recombina-

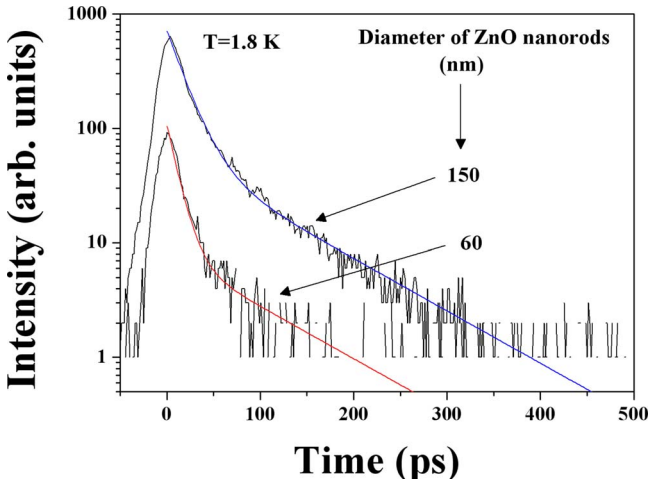

FIG. 3. (Color online) Decay curves for the CBD grown ZnO nanorods with two different diameters. The decays were measured at 1.8 K. The colored lines are fitted according to Eq. (1).

tion velocity S on decay time is determined by the diffusion equation with the proper boundary conditions.[28–30] In the one-dimensional case,[28] the carriers generated by the laser pulse start out with the following spatial distribution:

$$n(x,0) = \frac{N_0\alpha_\lambda(1-R)(e^{-\alpha_\lambda(x+d/2)} + \mathrm{Re}^{-\alpha_\lambda d}e^{-\alpha_\lambda(-x+d/2)})}{1-(\mathrm{Re}^{-\alpha_\lambda d})^2}.$$

Subsequently decay and diffusion of carriers were determined by the diffusion equation

$$\frac{\partial n}{\partial t} = D\frac{\partial n^2}{\partial x^2} - \frac{n}{\tau_B},$$

with boundary condition at two surfaces ($x=0$ and $x=d$),

$$D\left.\frac{\partial n}{\partial x}\right|_{x=0} = Sn|_{x=0},$$

$$-D\left.\frac{\partial n}{\partial x}\right|_{x=d} = Sn|_{x=d},$$

where N_0,α_λ, and R are the initial laser-pulse generated carriers, absorption coefficient constant at excitation laser wavelength λ, and reflection coefficient, respectively. τ_B is the decay time constant of bulk materials. In the nanorod case, the above diffusion equation and boundary conditions become three-dimensional equations. When the surface recombination is neglected, from the equation above, a single exponential decay with a time constant τ_B is expected.

We would like to point out that the situation is different for ZnO nanorods grown at high temperatures using the VLS growth. In this case, the surface recombination can be neglected, and the decay curve follows a single exponential decay (not shown here), such as in the bulk ZnO case shown in the inset of Fig. 2. Therefore, the observed nonexponential decay of the ZnO nanorods in our case suggests that the surface recombination cannot be neglected.

From Fig. 3, it is also observed that the fast decay component decreases with decreasing diameter of the CBD grown ZnO nanorods. This is consistent with the increasing importance of the surface layer with a decreasing nanorod diameter, i.e., the fast decay component is strongly influenced by the surface recombination velocity. It should be pointed out that there is no quantum confinement in the nanorods presented here since the diameter of those ZnO nanorods are well above carrier confinement limits. The task to solve the three-dimensional diffusion equation for our nanorods without any approximation is very difficult. Here we first choose a phenomenological way to correlate the fast component (τ_S) in the decay curves with the surface recombination velocity S, and then we use a simplified model to simulate the surface recombination effect on the exciton decay time. By examining the decay curves obtained for our CBD grown ZnO nanorods with various diameters, we find that the decay curves can be fitted by two exponential decays,

$$I(t) = A_S e^{-t/\tau_S} + A_B e^{-t/\tau_B}, \quad (1)$$

where $I(t)$ represents the PL intensity as a function of time, while A_S and A_B are the relative weights of the two exponential decays with time constants τ_S and τ_B, respectively.

The colored lines in Fig. 3 represent the fitting decay curves according to Eq. (1). The results show that the value of τ_B is the same, 95 ps, for all decay curves. We believe that this time constant represents an effective "bulk" exciton decay time in these nanorods. The same deduced value of τ_B for these nanorods with different diameters is not surprising since they were prepared under similar conditions. The deduced value for time constant τ_S and the ratio of A_S/A_B are summarized in Fig. 4. As seen in Fig. 4, τ_S decreases with the decreasing diameter of the nanorods while the ratio, A_S/A_B, increases. These factors indicate that the first term in Eq. (1) becomes more important in the influence of the decay time with decreasing nanorod sizes. It clearly illustrates that the surface effect becomes more important with decreasing diameter of our CBD grown ZnO nanorods. One should note that the surface recombination velocity should not change for samples prepared under similar conditions. However, the decay lifetime is influenced by the surface recombination velocity combined with the carrier diffusion length, resulting in a direct correlation with the size of the nanorods. This correlation will directly be reflected in the time constant τ_S introduced here.

In order to further explore how the surface recombination influences the first term in Eq. (1), an annealing procedure was performed. There are no observed changes concerning the diameter and the nanorod shape in the SEM images from the as-grown and thermal treated ZnO nanorods in the temperature used in this study. Figure 5 shows the effect of annealing on the recombination decay at a relative low temperature of 500 °C. In comparison with the as-grown sample, the value of τ_S and the ratio of A_S/A_B show a strong change (see Fig. 4), while the value of τ_B remains unchanged. The unchanged value for τ_B is consistent with the observation that only the near bandgap emission was enhanced by about a factor of 3 after the thermal treatment, while the deep level defect emission around 510 nm in the PL spectrum remained unchanged. The value of τ_S increases and the ratio of A_S/A_B decreases after the thermal treatment. This fact is consistent with an improvement of the surface

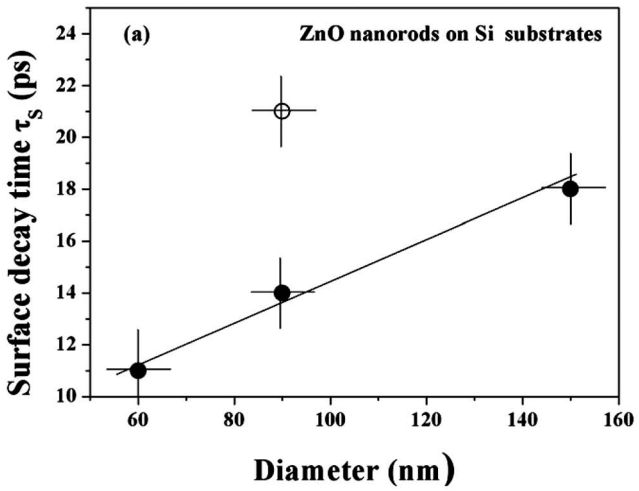

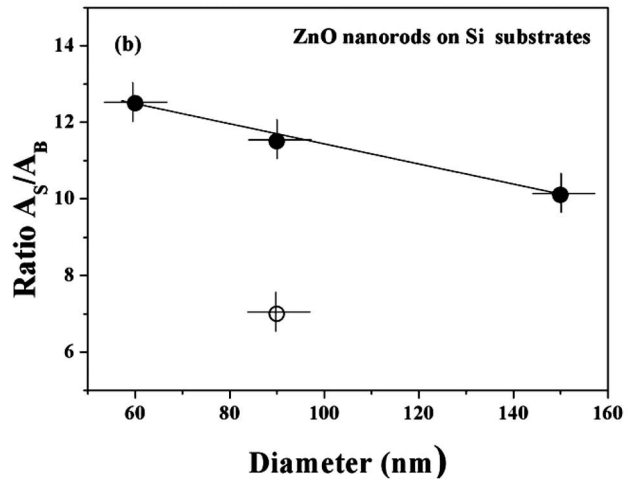

FIG. 4. (a) The deduced surface recombination times τ_s. (b) The deduced ratio A_S/A_B vs the diameter of the CBD grown ZnO nanorods according to Eq. (1). The corresponding data deduced from the annealed nanorods (open circle) are also included for comparison.

properties after the thermal treatment since the CBD grown ZnO nanorods are expected to have various chemicals attached to the surface due to the relatively low growth temperature (93 °C) and the nature of the CBD method. The mild thermal treatment will release the chemicals from the nanorod surfaces; consequently, the surface recombination is suppressed. In our samples, the bulk decay time in the ZnO nanorods remains unchanged after the mild thermal treatment.

In order to simplify the simulation according to a three-dimensional diffusion equation, we approximate the hexagonal shape of the ZnO nanorods with a cylinder shape. After the excitation by laser pulse, we have both free electrons and holes of density $n(\mathbf{r},t)$ and excitons of density $n_{ex}(\mathbf{r},t)$. We let the diffusion coefficient for the free particles and excitons be D and D_{ex}, respectively. The last diffusion coefficient we have found is negligible but we keep it here for completeness. The density of the free particles decays within the bulk with decay time τ_{B1} and via a surface channel with the surface decay velocity S. In both these processes the particles form excitons. The excitons go through radiative recombination processes in the bulk with decay time $\tau_{\mathrm{ex},B}$ or at the surface with the surface recombination velocity S_{ex}. The two densities are coupled via the following two coupled differential equations:

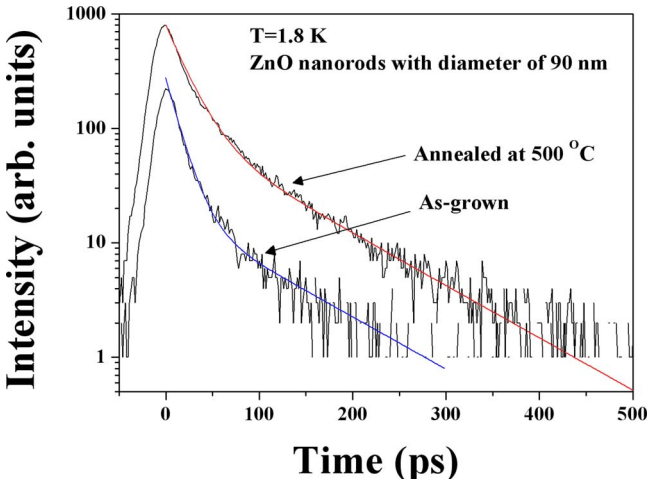

FIG. 5. (Color online) Decay curves for 90 nm diameter ZnO nanorods from as-grown sample and after annealing at 500 °C for 60 min. The decays were measured at 1.8 K. The colored lines are fitted according to Eq. (2).

$$\frac{\partial n(\mathbf{r},t)}{\partial t} = D\nabla^2 n(\mathbf{r},t) - \frac{n(\mathbf{r},t)}{\tau_{B1}},$$

$$\frac{\partial n_{\mathrm{ex}}(\mathbf{r},t)}{\partial t} = D_{\mathrm{ex}}\nabla^2 n_{\mathrm{ex}}(\mathbf{r},t) - \frac{n_{\mathrm{ex}}(\mathbf{r},t)}{\tau_{\mathrm{ex},B}} + \frac{n(\mathbf{r},t)}{\tau_{B1}}, \tag{2}$$

and fulfill the boundary conditions

$$-D \left.\frac{\partial n(\mathbf{r},t)}{\partial r}\right|_{r=R_0} = Sn(\mathbf{r},t)|_{r=R_0},$$

$$-D_{\mathrm{ex}} \left.\frac{\partial n_{\mathrm{ex}}(\mathbf{r},t)}{\partial r}\right|_{r=R_0} = S_{\mathrm{ex}} n_{\mathrm{ex}}(\mathbf{r},t)|_{r=R_0} - Sn(\mathbf{r},t)|_{r=R_0}.$$

We have used the values 10.8 cm^2/s and 25 ps for D and τ_{B1}, respectively, consistent with the experimental findings.[31] The exciton decay time $\tau_{\mathrm{ex},B}$ is about 95 ps in our case. We have discretized the problem by dividing the cylindrical pillars into 100 shells of equal thickness. The problem has been solved with iteration. The large value for the diffusion coefficient for the free carriers has forced us to use 10×10^6 time steps to cover 250 ps. At each step free carriers are diffusing into and out of each shell. Some of the free carriers are leaving by forming excitons. Some of the excitons are leaving through bulk recombination; some are entering from the process where the free carriers are forming excitons. In the outer shell there are the additional surface processes. We have assumed (as initial conditions) that there are no excitons and that the free carriers are homogeneously distributed throughout the pillars. In our simulations, we have used two free varying parameters, i.e., S_{ex} and S, since there are no information available concerning those two parameters in literature. The experimental decay curve for our 150 nm ZnO nanorods is shown together with calculated curves using different sets of values for S_{ex} and S in Fig. 6.

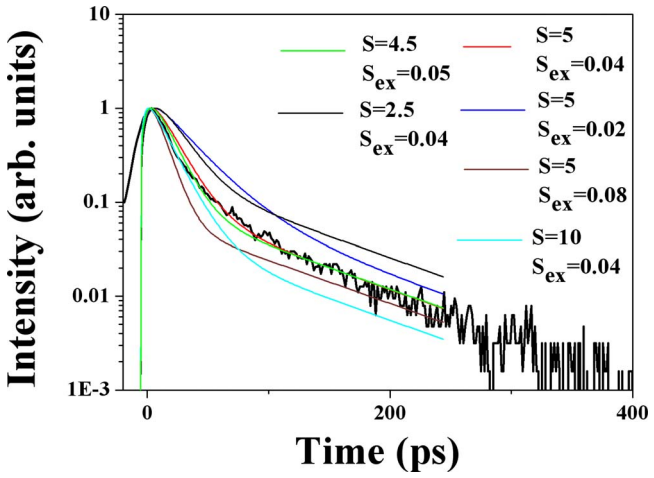

FIG. 6. (Color online) Decay curves for 150 nm diameter ZnO nanorods from as-grown sample and the calculated curves for various values of S_{ex} (nm/ps) and S (nm/ps).

The results clearly show the effect of S_{ex} and S, and the best fitting is obtained by using the parameters of $S_{ex}=0.05$ nm/ps and $S=4.5$ nm/ps. Through the same fitting procedure, we fitted the experimental results obtained for the 90 and 60 nm samples with parameters of $S_{ex}=0.05$ nm/ps and $S=2.5$ nm/ps and of $S_{ex}=0.05$ nm/ps and $S=1.5$ nm/ps, respectively. The results clearly indicate that we cannot use the same set of parameters to fit various diameter ZnO nanorods. We believe that this error is due to our approximation in our calculation, i.e., we approximate the hexagonal shape of the ZnO nanorods with a cylinder shape. Nevertheless, our simulations provide a magnitude and approximated value of the surface recombination velocity for ZnO nanorods. Figure 7 shows the results of surface decay time experimentally deduced in Fig. 4(a) and theoretically calculated by using Eq. (2). The two calculated curves by using the sets of parameters from 150 and 60 nm samples provide a tendency and a range of the surface decay time in the ZnO nanorod structures used in this study.

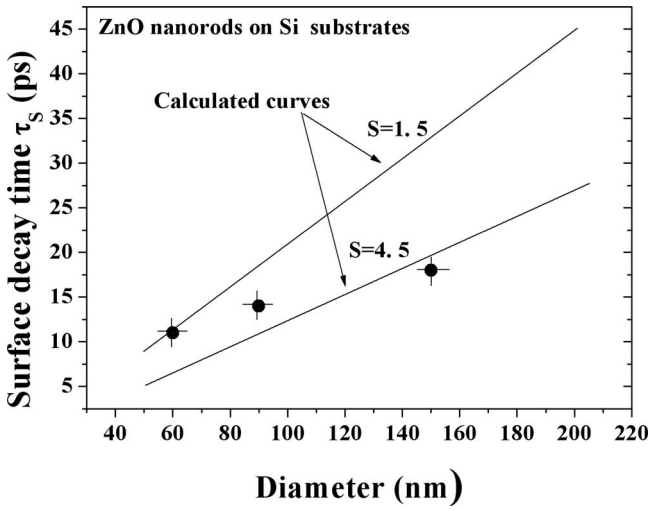

FIG. 7. The deduced surface recombination times τ_s and calculated curves. The S value is in nm/ps unit.

In summary, we have presented, for the first time, a time resolved PL study in CBD grown ZnO nanorods with different diameters. The results show that the decay time of the excitons in the nanorods strongly depends on the diameter of the nanorods. The altered decay time is mainly due to the surface recombination process. The effective time constant related to the surface recombination velocity was deduced. The results show that the time constant decreases with the decreasing diameter of the nanorods. A thermal treatment will suppress the surface recombination channel, resulting in an improvement of the optical quality for the ZnO nanorods. Although we have not been able to deduce the exact surface recombination velocity, we hope that our results will stimulate more theoretical and experimental investigations of the surface recombination processes in nanostructures.

ACKNOWLEDGMENTS

The authors would like to acknowledge financial support from the Swedish Research Council (VR) and financial support through NANDOS project from European Commission.

[1] M. W. Cho, A. Setiawan, H. J. Ko, S. K. Hong, and T. Yao, Semicond. Sci. Technol. **20**, S13 (2005).
[2] T. Ohgaki, N. Ohashi, H. Kakemoto, S. Wada, Y. Adachi, H. Haneda, and T. Tsurumi, J. Appl. Phys. **93**, 1961 (2003).
[3] Y. Chen, D. M. Bagnall, H.-J. Koh, K.-T. Park, K. Hiraga, Z.-Q. Zhu, and T. Yao, J. Appl. Phys. **84**, 3912 (1998).
[4] A. Bakin, A. El-Shaer, A. Che Mofor, M. Kreye, A. Waag, F. Bertram, J. Christen, M. Heuken, and J. Stoimenos, J. Cryst. Growth **287**, 7 (2006).
[5] J. M. Pierce, B. T. Adekore, R. F. Davis, and F. A. Stevie, J. Cryst. Growth **277**, 345 (2005).
[6] W. I. Park, G. C. Yi, M. Kim, and S. J. Pennycook, Adv. Mater. (Weinheim, Ger.) **15**, 526 (2003).
[7] A. Dadgar, N. Oleynik, D. Forster, S. Deiter, H. Witek, J. Blasing, F. Bertram, A. Krtschil, A. Diez, J. Christen, and A. Krost, J. Cryst. Growth **267**, 140 (2004).
[8] M. Pan, W. E. Fenwick, M. Strassburg, N. Li, H. Kang, M. H. Kane, A. Asghar, S. Gupta, R. Varatharajan, J. Nause, N. El-Zein, P. Fabiano, T. Steiner, and I. Ferguson, J. Cryst. Growth **287**, 688 (2006).
[9] A. Dadgar, N. Oleynik, D. Forster, S. Deiter, H. Witek, J. Bläsing, F. Bertram, A. Krtschil, A. Diez, J. Christen, and A. Krost, J. Cryst. Growth **267**, 140 (2004).
[10] Y. Zhang, G. Du, H. Zhu, C. Hou, K. Huang, and S. Yang, Opt. Mater. (Amsterdam, Neth.) **27**, 399 (2004).
[11] W. Prellier, A. Fouchet, Ch. Simon, and B. Mercey, Mater. Sci. Eng., B **109**, 192 (2004).
[12] E. McGlynn, J. Fryar, G. Tobin, C. Roy, M. O. Henry, J. P. Mosnier, E. de Posada, and J. G. Lunney, Thin Solid Films **458**, 330 (2004).
[13] Z. L. Wang, Annu. Rev. Phys. Chem. **55**, 159 (2004).
[14] Z. L. Wang, Mater. Today **7**, 26 (2004).
[15] Q. X. Zhao, P. Klason, and M. Willander, Appl. Phys. A: Mater. Sci. Process. **88**, 27 (2007).
[16] F. Chaabouni, M. Abaab, and B. Rezig, Sens. Actuators B **100**, 200 (2004).
[17] R. B. Peterson, C. L. Fields, and B. A. Gregg, Langmuir **20**, 5114 (2004).
[18] H. D. Yu, Z. P. Zhang, M. Y. Han, and X. T. Hao, J. Am. Chem. Soc. **127**, 2378 (2005).
[19] C. H. Hung and W. T. Whang, J. Cryst. Growth **268**, 242 (2004).
[20] D. G. Kim, S. Wakaiki, S. Komura, M. Nakayama, Y. Mori, and K. Suzuki, Appl. Phys. Lett. **90**, 101918 (2007).
[21] W. I. Park, D. H. Kim, S.-W. Jung, and G.-C. Yi, Appl. Phys. Lett. **80**, 4232 (2002).
[22] W. I. Park, Y. H. Jun, S. W. Jung, and G.-C. Yi, Appl. Phys. Lett. **82**, 964 (2003).
[23] J. Jie, G. Wang, Y. Chen, X. Han, Q. Wang, B. Xu, and J. G. Hou, Appl. Phys. Lett. **86**, 031909 (2005).
[24] W. Lee, M.-C. Jeong, and J.-M. Myoung, Appl. Phys. Lett. **85**, 6167 (2004).

[25]I. C. Robin, B. Gauron, P. Ferret, C. Tavares, G. Feuillet, L. S. Dang, B. Gayral, and J. M. Gérard, Appl. Phys. Lett. **91**, 143120 (2007).
[26]A. Mézy, S. Anceau, T. Bretagnon, P. Lefebvre, T. Taliercio, G.-C. Yi, and J. Yoo, Superlattices Microstruct. **39**, 358 (2006).
[27]L. L. Yang, Q. X. Zhao, and M. Willander, J. Alloys Compd. (in press).
[28]K. L. Luke and L.-J. Cheng, J. Appl. Phys. **61**, 2282 (1987).
[29]A. Buczkowski, Z. J. Radzimski, G. A. Rozgonyi, and F. Shimura, J. Appl. Phys. **69**, 6495 (1991).
[30]K. Thölmann, M. Yamaguchi, A. Yahata, and H. Ohashi, Jpn. J. Appl. Phys., Part 1 **32**, 1 (1993).
[31]J. Takeda, K. Takagi, T. Okabe, H. J. Ko, and T. Yao, Phys. Status Solidi C **1**, 678 (2004).